Acta Crystallographica Section B
Structural Science
ISSN 0108-7681

Reproducability and transferability of topological properties; experimental charge density of the hexapeptide cyclo-(D,L-Pro)$_2$–(L-Ala)$_4$ monohydrate

B. Dittrich,[a] T. Koritsánszky,[b] M. Grosche,[c] W. Scherer,[c] R. Flaig,[a] A. Wagner,[a] H. G. Krane,[d] H. Kessler,[e] C. Riemer,[e] A. M. M. Schreurs[f] and P. Luger[a]*

[a]Institut für Chemie/Kristallographie der Freien Universität Berlin, D-14195 Berlin, Germany, [b]Department of Chemistry, State University of New York at Buffalo, Buffalo, NY 14260, USA, [c]Anorganisch-chemisches Institut der TU München, D-85747 Garching bei München, Germany, [d]Mineralogisch-Petrologisches Institut, Universität Bonn, Poppelsdorfer Schloss, D-53115 Bonn, Germany, [e]Institut für Organische Chemie und Biochemie, Lehrstuhl II der TU München, Lichtenbergstrasse 4, D-85747Garching bei München, Germany, and [f]Department of Crystal and Structural Chemistry, Bijvoet Centre for Biomolecular Research, Padulaan 8, Utrecht, NL-3584, The Netherlands

Correspondence e-mail: luger@chemie.fu-berlin.de

Received 22 February 2002
Accepted 2 April 2002

The charge density of a hexapeptide was determined from high-resolution CCD area-detector experiments at 100 K. Two datasets, one from a rotating anode and a second one from synchrotron radiation, were measured and the results are compared. The data are interpreted in terms of the 'rigid pseudoatom' model. The topology of the experimental density is analyzed and compared with the topology of the constituting amino acids, and shows good agreement. All critical points of the electron density at the covalent and hydrogen bonds, as well as those of the Laplacian, were located. With respect to the transferability of electronic and bond topological properties the six peptide bonds were compared with values given in the literature.

1. Introduction

An important implication of Bader's theory of atoms in molecules (Bader, 1994) is the partitioning of a chemical structure into submolecular or atomic fragments and the question of transferability of topological properties from these fragments to larger molecules. Chang & Bader (1992) as well as Popelier & Bader (1994) have recently addressed these questions to oligopeptides and several other molecules such as *e.g.* pyridine (Bader & Bayles, 2000) using theoretical calculations.

Lecomte and co-workers have investigated the effect of a transfer of multipole populations of amino acids, pseudopeptides and oligopeptides to larger systems (Jelsch *et al.*, 1998; Pichon-Pesme & Lecomte, 1998; Dahaoui *et al.*, 1999). They have also compared different topological properties of several di-, tri- and pseudopeptides (Benabicha *et al.*, 2000).

In general, topological properties such as the electron density $\rho(\mathbf{r}_b)$, the Laplacian $\nabla\rho(\mathbf{r}_b)$ and the ellipticity ϵ at the bond critical point [defined by the condition that $\nabla\rho(\mathbf{r}_b) = 0$] are accessible from the three-dimensional distribution of electron density $\rho(\mathbf{r})$, which can be determined theoretically from an *ab initio* calculation or experimentally from a high-resolution X-ray diffraction experiment at low temperatures.

Owing to the introduction of area detectors (CCD or image plate) in combination with an intense X-ray source (Koritsánszky *et al.*, 1998), the time-consuming single-crystal X-ray experiment can now be performed within one or a few days. Charge density studies are now possible for a whole class of chemically related compounds or on larger molecules.

After we have shown that experimentally determined topological properties at the bond critical points $\mathbf{r}_b$ of several amino acids exhibit a high degree of transferability (Flaig *et al.*, 1999, 2002) the title compound, the hexapeptide *cyclo*-(D,L-Pro)$_2$–(L-Ala)$_4$ monohydrate (Fig. 1), provides the chance to examine the transferability of chemically equivalent bonds

Table 1
Crystal and structure refinement data for cyclo-(D,L-Pro)$_2$–(L-Ala)$_4$ monohydrate.

Empirical formula	$C_{22}H_{34}N_6O_6\cdot H_2O$	
Formula weight (g mol^{-1})	496.56	
Crystal system	Orthorhombic	
Space group	$P2_12_12_1$ (No. 19)	
Z	4	
Temperature (K)	100 (1)	
Dataset	Synchrotron	Rotating anode
Unit-cell dimensions		
a (Å)	10.128 (1)	10.127 (1)
b (Å)	12.486 (1)	12.501 (1)
c (Å)	19.507 (1)	19.495 (1)
V (Å^3)	2466.8 (4)	2467.8 (4)
Calculated density (g cm^{-3})	1.337	1.336
$F(000)$	1064.0	
λ (Å)	0.5583	0.7107
Absorption coefficient μ (mm^{-1})	0.06	0.10
Max. 2θ (°)	94.96	107.26
$(\sin\theta/\lambda)_{max}$ (Å^{-1})	1.32	1.13
No. of collected reflections	185 339	293 943
No. of symmetry-independent reflections	45 772	29 731
Completeness (%)	98.5	98.8
Redundancy after integration	7.45	9.89
$R_{int}(F^2)$	0.064	0.036
$R_w(F)$	0.027	0.030
$R_1(F)$	0.025	0.020
$R_{all}(F)$	0.031	0.027
Gof	1.41	1.62

$R_{int}(F^2) = \sum|F_o^2 - F_o^2(\text{mean})|/\sum F_o^2$, $R_w(F) = [\sum w||F_o| - k|F_c||^2/\sum w|F_o|^2]^{1/2}$, $w = 1/\sigma^2$, $R_1(F) = \sum||F_o| - |F_c||/\sum|F_o|$, $R_{all}(F)$ using all reflections, Gof = $[\sum||F_o| - k|F_c||^2/(n_o - m_{var})]^{1/2}$.

on a larger oligopeptide molecule. It consists of amino acids on which the experimental charge density is known (Koritsánszky *et al.*, 1998; Gatti *et al.*, 1992). Additionally it allows the comparison of the six peptide bonds. A further aspect of topological studies of oligopeptides is that they may contain submolecular fragments that are part of compounds of high biological importance. The penicillines, for example, act as a substrate analog of the terminal alanyl–alanine fragment of an oligopeptide, which plays a major role in the bacterial cell wall synthesis. This hexapeptide, including a tetraalanine fragment, contains three different Ala–Ala conformations and can therefore be used for comparative purposes in the charge density study of penicillines, which is under investigation in our laboratory (Wagner *et al.*, 2000).

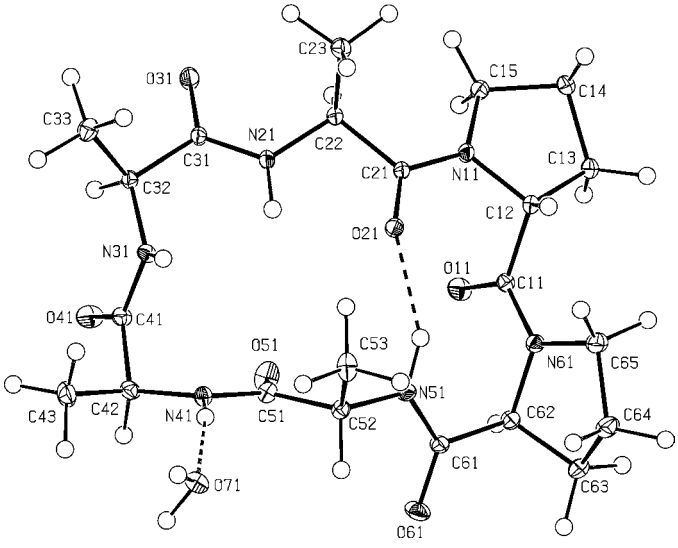

Figure 1
ORTEP representation (Burnett & Johnson, 1996) of the experimentally determined molecular structure in the crystal with atomic numbering scheme; thermal ellipsoids with 50% probability.

2. Experimental

Two CCD datasets, one using synchrotron radiation, the other one a rotating anode, were collected. With synchrotron radiation (beamline D3, Hasylab/DESY) 185 339 reflections were measured on 13 308 frames within 3 d up to a resolution of $\sin\theta/\lambda$ = 1.32 Å^{-1} and an almost complete coverage (98.5%) of the reciprocal space at a wavelength of λ = 0.5583 Å. The decay of the synchrotron radiation was monitored and corrected. The experimental setup consisted of a Huber four-circle diffractometer and a Bruker SMART 1K CCD detector; the temperature of the experiment was maintained at 100 K using an Oxford cryosystem nitrogen gas stream cooling device. The measurement strategy was planned using *ASTRO*; the *SMART* and *SAINT* routines were used for data collection and integration; *SADABS* was used for correction (Bruker AXS Inc., 1994–1996).

The redundancy of data is even higher for the rotating-anode dataset. Here, 293 943 reflections were collected up to a resolution of $\sin\theta/\lambda$ = 1.13 Å^{-1} with a coverage of 98.9%. A Nonius FR 591 rotating anode with a Kappa CCD system and an Oxford cryosystem nitrogen gas stream cooling device (100 K) were used. *EVAL* (Nonius, 2000) and *SORTAV* (Blessing, 1995) programs were applied for integration and absorption correction. Further details on the crystal data and the conditions for both experiments are given in Table 1.[1]

3. Density models and refinement strategy

Both datasets were refined using the Hansen and Coppens multipole formalism (Hansen & Coppens, 1978), as implemented in the program package *XD* (Koritsánszky *et al.*, 1995) using identical models for both datasets. It allows a modelling of the aspherical fraction of $\rho(\mathbf{r})$ using atom-centered multipole functions,

$$\rho_{atom}(\mathbf{r}) = \rho_{core}(r) + P_v\kappa'^3\rho_{valence}(\kappa' r) + \rho_{deformation} \qquad (1)$$

with

$$\rho_{deformation} = \sum_{l=0}^{4}\kappa''^3 R_l(\kappa''\mathbf{r})\sum_{m=0}^{l}P_{lm\pm}Y_{lm\pm}(\theta,\varphi).$$

The starting atomic parameters were taken from the spherical atom refinement (*SHELXL*; Sheldrick, 1997). In the multipole

[1] Supplementary data for this paper are available from the IUCr electronic archives (Reference: LC0050). Services for accessing these data are described at the back of the journal.

Table 2
Comparison of the electron density, the Laplacian and the ellipticity for the peptide linkages.

	Synchrotron			Rotating anode			B3LYP 6-311++G(3d,3p)		
	$\rho(\mathbf{r}_b)$	$\nabla^2\rho(r_b)$	ϵ	$\rho(r_b)$	$\nabla^2\rho(r_b)$	ϵ	$\rho(r_b)$	$\nabla^2\rho(r_b)$	ϵ
N11—C21 P–A	2.44 (3)	−26.1 (1)	0.30	2.36 (4)	−24.1 (1)	0.22	2.29	−25.9	0.18
N21—C31 A–A	2.51 (2)	−26.3 (1)	0.16	2.36 (2)	−26.8 (1)	0.21	2.29	−25.8	0.15
N31—C41 A–A	2.43 (2)	−23.4 (1)	0.16	2.30 (2)	−24.0 (1)	0.21	2.21	−24.4	0.14
N41—C51 A–A	2.43 (2)	−23.3 (1)	0.16	2.29 (2)	−23.5 (1)	0.21	2.20	−24.5	0.14
N51—C61 A–P	2.46 (3)	−20.2 (1)	0.15	2.49 (4)	−27.5 (1)	0.37	2.32	−26.4	0.16
N61—C11 P–P	2.40 (2)	−23.0 (1)	0.19	2.21 (4)	−21.7 (1)	0.30	2.21	−24.2	0.18
	2.4(1)†	−26 (4)	0.1						

$\rho(\mathbf{r}_b)$ (in e Å^{-3}) and $\nabla^2\rho(\mathbf{r}_b)$ (in e Å^{-5}) denote the electron density and the Laplacian at the bond critical point $\mathbf{r}_b$. ϵ is the bond ellipticity. † Mean value from Pichon-Pesme *et al.* (2000).

Table 3
Intra- and intermolecular contacts indicating possible hydrogen bonds and their bond topological parameters.

$\rho(\mathbf{r}_b)$ is in e Å^{-3}, $\nabla^2\rho(\mathbf{r}_b)$ in e Å^{-5}. *D* denotes the donating, *A* the accepting atom. *D*—H distances (in Å) were set to the given values.

D—H···*A*	*D*—H	H···*A*	*D*···*A*	*D*—H···*A*	$\rho(\mathbf{r}_b)$	$\nabla^2\rho(\mathbf{r}_b)$
O71—H71*A*···O61^{i}	0.95	1.7724	2.7195 (5)	174.46	0.15 (1)	5.8 (1)
O71—H71*B*···O31^{ii}	0.95	1.8970	2.8299 (5)	166.66	0.10 (1)	4.2 (1)
N41—H41···O71^{iii}	1.00	1.9374	2.9103 (4)	163.56	0.08 (1)	3.1 (1)
N51—H51···O21^{iii}	1.00	2.0023	2.9184 (3)	151.18	0.08 (1)	2.5 (1)
N31—H31···O41^{ii}	1.00	2.0196	3.0064 (4)	168.66	0.05 (1)	2.6 (1)
N21—H21···O21^{iii}	1.00	2.1825	2.6219 (3)	104.75	–	–
N51—H51···N61^{iii}	1.00	2.2982	2.7159 (3)	103.78	–	–
N21—H21···N31^{iii}	1.00	2.3628	2.7735 (3)	103.58	–	–
C32—H32···O41^{iii}	1.08	2.2628	2.7723 (4)	106.64	–	–
C52—H52···O61^{iii}	1.08	2.3633	2.7817 (4)	101.14	–	–
C12—H12···O11^{ii}	1.08	2.2427	3.2390 (4)	152.44	0.04 (1)	1.4 (1)
C32—H32···O71^{iv}	1.08	2.4546	3.2479 (4)	129.29	0.04 (1)	0.8 (1)
C13—H13*A*···O51^{ii}	1.08	2.5035	3.2824 (4)	128.14	–	–
C15—H15*A*···O71^{v}	1.08	2.4904	3.4018 (4)	141.38	0.03 (1)	0.7 (1)
C43—H43*A*···O61^{i}	1.08	2.5190	3.5250 (6)	154.57	0.02 (1)	0.6 (1)
C64—H64*A*···O31^{ii}	1.08	2.5527	3.5239 (5)	149.18	–	–
C53—H53*B*···O71^{iii}	1.08	2.5960	3.5319 (4)	144.55	0.02 (1)	0.6 (1)
C23—H23*B*···O71^{v}	1.08	2.5055	3.5714 (4)	168.91	0.01 (1)	0.7 (1)

Symmetry codes: (i) $1-x, -\frac{1}{2}+y, \frac{1}{2}-z$; (ii) $\frac{1}{2}+x, \frac{3}{2}-y, 1-z$; (iii) x, y, z; (iv) $-\frac{1}{2}+x, \frac{1}{2}-y, 1-z$; (v) $\frac{3}{2}-x, 1-y, \frac{1}{2}+z$.

formalism the core and the spherical valence density of the heavy atoms were composed of Hartree–Fock wavefunctions expanded over Slater-type basis functions. For the deformation terms single-zeta orbitals with energy-optimized Slater exponents were taken and kept fixed (Clementi & Roetti, 1974). In all cases the quantity $\Sigma_{\mathbf{H}} w_{\mathbf{H}}[|F_{\rm obs}(\mathbf{H})| - k|F_{\rm cal}(\mathbf{H})|]^2$ was minimized using the statistical weight $w_{\mathbf{H}} = \sigma^{-2}[F_{\rm obs}(\mathbf{H})]$. Additional to the positional and thermal parameters populations up to hexadecapoles for non-H atoms and bond-directed dipoles for H atoms (P_v and P_{lm}) were refined together with expansion/contraction parameters κ in the least-squares procedure. The symmetry $3m$ was imposed for the methyl groups (C23, C33, C43 and C53; for atomic numbering scheme see Fig. 1). Bonds to H atoms were set to the standard neutron distances. No charge transfer was allowed between the molecules and the total charge was kept constant. For the agreement factors see Table 1. The Hirshfeld test (Hirshfeld, 1976) shows that the highest difference of mean-squares displacement amplitudes was 0.0006 Å^2, indicating a proper deconvolution of thermal motion and electron density. No significant electron density was found in the residual density maps (Fig. 2) that include all reflections (no resolution cutoff).

In the least-squares module *XDLSM* of *XD* (Koritsánszky *et al.*, 1995) it is possible to constrain multipole parameters to be equal for chemically equivalent atoms. This procedure, like the assumption of local atomic site symmetry, reduces the number of parameters and increases the data/parameter ratio. Concerning transferability, chemical constraints could create the problem that too much prior information is entered into a system. Two multipole models were therefore considered and compared. The first model does not make use of chemical constraints. Data presented here are based on a second model that cautiously uses constraints for the alanine and the proline fragments. Both models do not differ significantly and show similar residual and deformation density as well as figures of merit.

4. Theoretical calculations

The program package *GAUSSIAN*98 (Frisch *et al.*, 1998) was used for a single-point density functional calculation based on the experimental geometry with the basis set B3LYP/6-311++G(3d,3p). The wavefunction obtained was evaluated with the program *AIMPAC* (Cheeseman *et al.*, 1992).

5. Results and discussion

Fig. 3 shows static deformation density maps in the plane of the six peptide bonds. They show, apart from the good figures of merit and the low residual electron density, the proper representation of $\rho(\mathbf{r})$ by the model. In all cases covalent bonds and lone-pair regions indicate a similar distribution of electron density concerning shape and intensity. The electrostatic potential (Fig. 4, same orientation as in Fig. 1) reveals a large negative region around the alanine fragments and a positive potential in the proline part, so that a charge separation between the proline and alanine residues is visible.

To compare topological properties the same atoms in a similar chemical environment are considered. The C_α atom in oligopeptides differs from the C_α atom in amino acids as the carboxylate and amino functional groups form the backbone in an oligopeptide. Thus they are not comparable to the monomer, in contrast to the side chains. Table 2 lists values for topological properties of the six peptide bonds of the hexapeptide of both measurements. They are compared with the mean value from the literature (Pichon-Pesme *et al.*, 2000) and results from the above-mentioned density functional calculation based on the rotating-anode experimental geometry.

For values of $\rho(\mathbf{r}_b)$ or the Laplacian $\nabla^2\rho(\mathbf{r}_b)$ at the bond critical point $\mathbf{r}_b$ we find differences of 0.1 e Å^{-3} or 2 e Å^{-5} for both datasets. These values are just in the range that Lecomte and co-workers have reported for a number of experimental studies on pseudopeptides (Pichon-Pesme *et al.*, 2000; see also quantitative results from Table 2), so that this seems to be the possible reproducibility of experimental charge density studies.

Table 4 compares $\rho(\mathbf{r}_b)$ and $\nabla^2\rho(\mathbf{r}_b)$ of side-chain bonds of the hexapeptide with those of the corresponding building block amino acids L-alanine and DL-proline. Here the agreement for the $C_\alpha-C_\beta$, $C_\beta-C_\gamma$ or $C_\alpha-N$ single bonds between experiment and theory as well as between the two experiments is very good, so transferability for topological parameters can be concluded for the side chains.

In Table 3 the topological data for the weak interactions are summarized. Considering geometry criteria alone, several intra- and intermolecular hydrogen bonds are indicated (Spek, 1990). According to Bader (1994), an attractive interaction between two atoms is a path with maximum charge density $\rho(\mathbf{r})$ linking

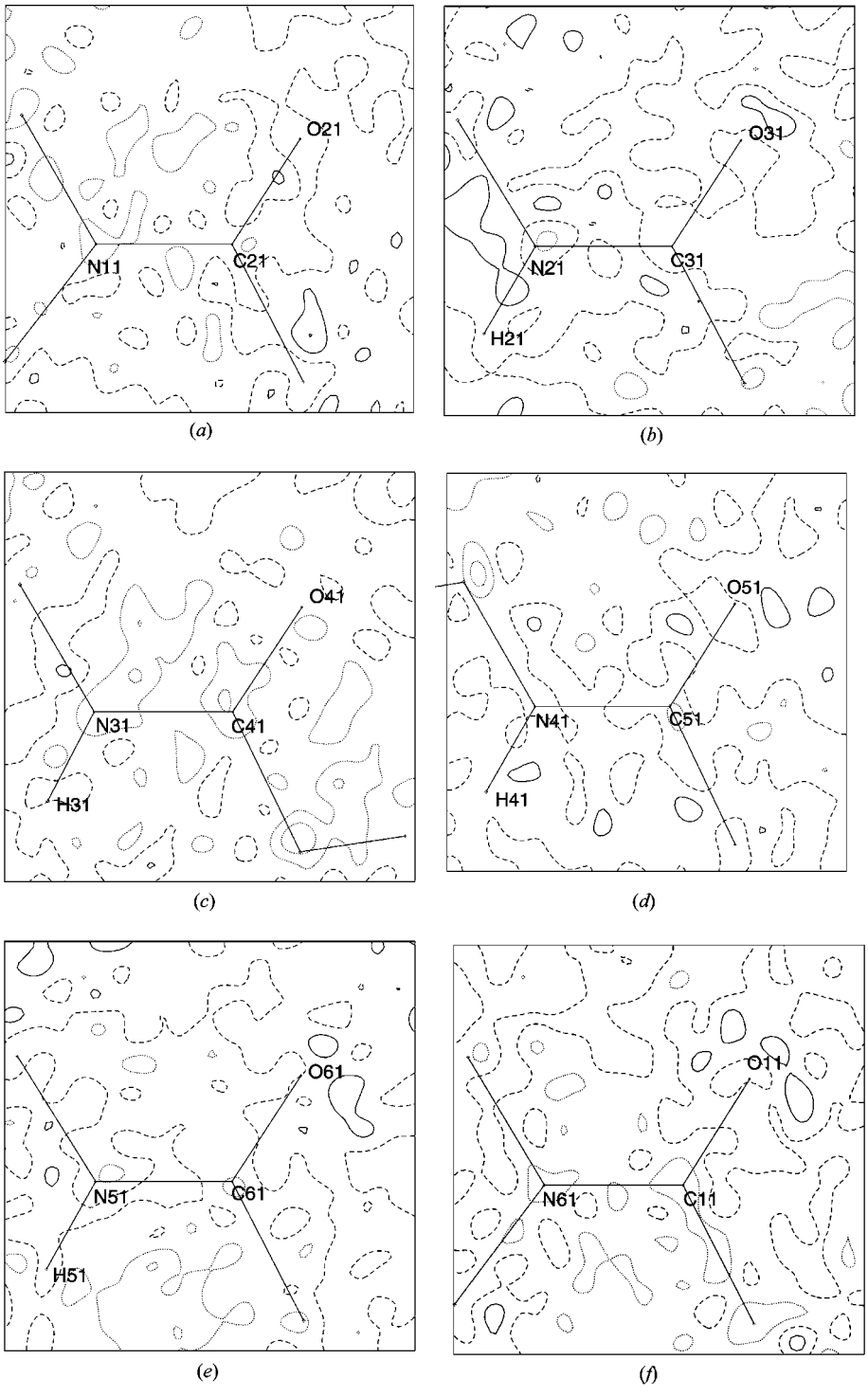

Figure 2
Residual density maps (synchrotron data) in the planes of the six peptide bonds. Upper left to bottom right: D-Pro–Ala_1, Ala_1–Ala_2, Ala_2–Ala_3, Ala_3–Ala_4, Ala_4–L-Pro, L-Pro–D-Pro. Contour lines (full lines = positive, dotted = negative) are 0.1 e Å^{-3}; zero line dashed. No resolution cut-off.

two nuclei, characterized by a (3,−1) bond critical point. Examining the weak interactions in detail reveals that for some of them no bond critical point is found. There are three such groups of interactions to consider; the first one is a N—H···X (with X = N, O) case, where the ring structure and the rigid peptide bond forces N21—H21···O21, N21—H21···N31 and N51—H51···N61 to close contacts. The second group are the close C_α—H···O contacts C32—H32···O41 and C52—H52···O61. Finally, the methyl H atom in C64—H64*A*···O31 is also forced to be close to an O atom. While for none of them a critical point was found, this was the case for some further C—H···O interactions, as shown in Table 3. Topological analysis helps to differentiate between problem cases and allows to quantify the strength of these hydrogen bonds.

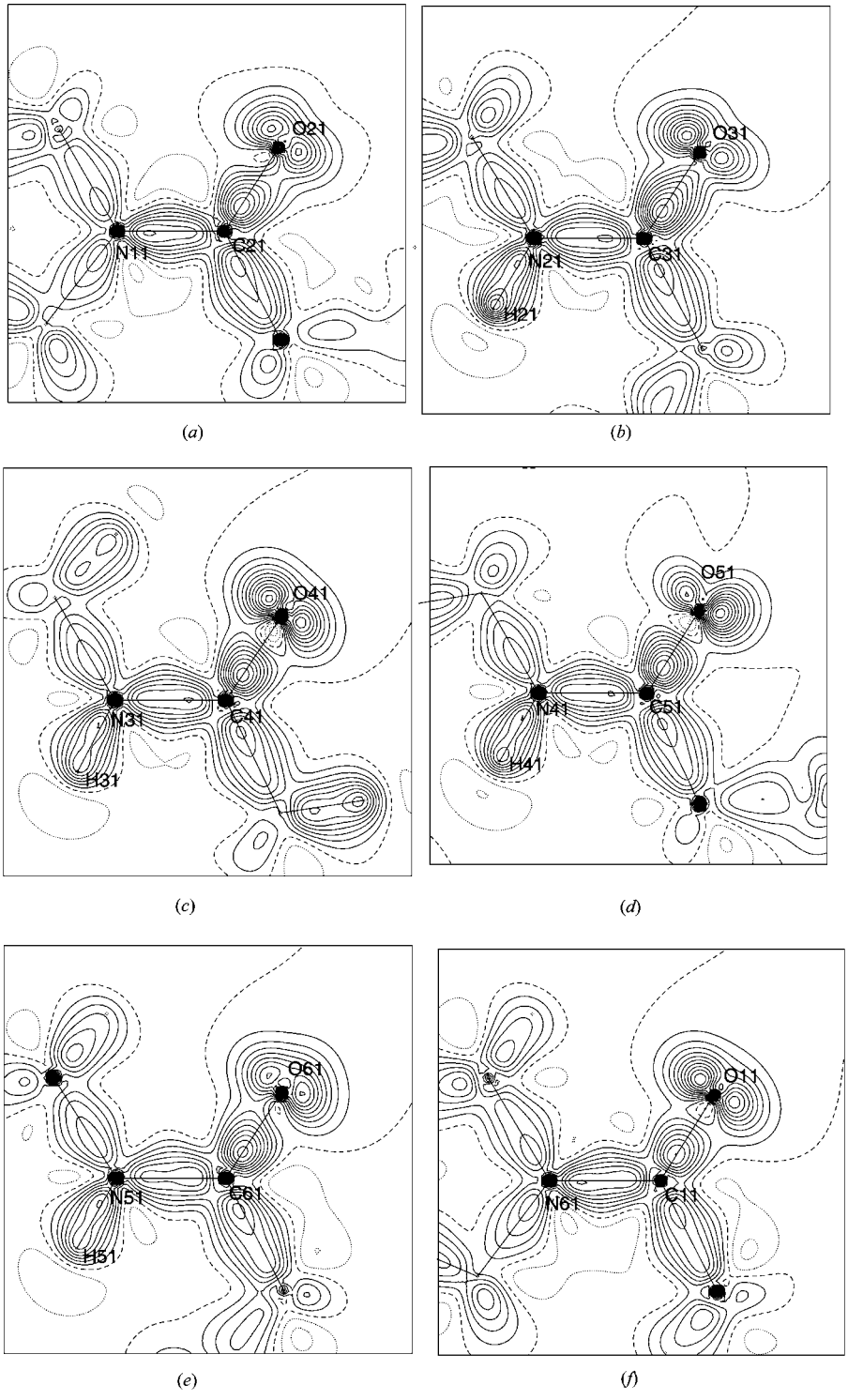

Figure 3
Static experimental deformation density maps (synchrotron data) in the plane of the six peptide bonds. Upper left to bottom right: D-Pro–Ala_1, Ala_1–Ala_2, Ala_2–Ala_3, Ala_3–Ala_4, Ala_4–L-Pro, L-Pro–D-Pro. Contour lines (full lines = positive, dotted = negative) are 0.1 e Å^{-3}; zero line dashed.

Espinosa *et al.* (1998) have investigated the correlation between hydrogen-bond strength (the density and the Laplacian found at the bond critical point) and the hydrogen–acceptor distance and found an exponential behaviour. Spackman (1999) has shown that except for very strong interactions this can also be described by the promolecule alone. The hydrogen bonds of the title compound agree with these findings and also show the exponential behaviour described.

The hydrogen-bonding pattern influences the lone-pair density. Table 5 shows the results for a lone-pair search around the O atoms. The distances of the maxima to their parent O atoms and the electron density, as well as the values of the Laplacian function at these points, compare very well with earlier findings for the dipeptide glycyl-L-threonine dihydrate (Dittrich *et al.*, 2000). If the positions of the (3,+3) critical points are considered with respect to the O atoms and the corresponding hydrogen-bond critical points, it turns out that the (3,+3) critical points are rearranged in directions towards the H atom that they accept. The strength and number of weak interactions seem to be correlated with the amount of lone-pair electron density. The strongest hydrogen bond is formed by O71, which donates one of its H atoms to O61 of a neighboring hexapeptide molecule. O71 also has the weakest lone pair. The sum of both lone-pair densities is smaller for O atoms that are involved in hydrogen bonding (O21, O31, O61 and O71), whereas for O41, that accepts just one very weak C—H···O

Table 4
Comparison of the electron density $\rho(\mathbf{r}_b)$ and the Laplacian $\nabla^2\rho(\mathbf{r}_b)$ at the bond critical point $\mathbf{r}_b$ for the side chains.

$\rho(\mathbf{r}_b)$ is in e Å^{-3}, $\nabla^2\rho(\mathbf{r}_b)$ in e Å^{-5}.

		Synchrotron		Rotating anode	
		$\rho(\mathbf{r}_b)$	$\nabla^2\rho(\mathbf{r}_b)$	$\rho(\mathbf{r}_b)$	$\nabla^2\rho(\mathbf{r}_b)$
Cyclo-(D,L-Pro)$_2$-(L-Ala)$_4$	C12—C13	1.62 (2)	−8.0 (1)	1.61 (1)	−10.9 (1)
	C13—C14	1.65 (2)	−11.2 (1)	1.55 (1)	−8.8 (1)
	C14—C15	1.74 (2)	−12.7 (1)	1.72 (1)	−11.3 (1)
Prolin 1	C15—N11	1.76 (2)	−10.9 (1)	1.74 (1)	−13.1 (1)
Cyclo-(D,L-Pro)$_2$-(L-Ala)$_4$	C62—C63	1.65 (2)	−8.4 (1)	1.64 (1)	−11.3 (1)
	C63—C64	1.71 (1)	−13.1 (1)	1.66 (1)	−10.4 (1)
	C64—C65	1.64 (2)	−10.2 (1)	1.57 (1)	−9.0 (1)
Prolin 2	C65—N61	1.74 (1)	−10.5 (1)	1.72 (1)	−12.7 (1)
DL-Prolin†	C2—C3	1.66 (2)	−11.6 (1)		
	C3—C4	1.64 (2)	−12.0 (1)		
	C4—C5	1.75 (2)	−15.9 (1)		
	C5—N1	1.70 (2)	−8.2 (1)		
Cyclo-(D,L-Pro)$_2$-(L-Ala)$_4$	C22—C23	1.64 (1)	−9.8 (1)	1.63 (1)	−8.9 (1)
	C32—C33	1.65 (1)	−10.0 (1)	1.64 (1)	−9.0 (1)
	C42—N43	1.65 (1)	−10.0 (1)	1.63 (1)	−8.9 (1)
Alanin 1-4	C52—N53	1.66 (1)	−10.3 (1)	1.65 (1)	−9.2 (1)
L-Alanin‡	C2—C3	1.66 (2)	−11.6 (1)		

† Data from Koritsánszky *et al.* (1998). ‡ Data from Gatti *et al.* (1992).

hydrogen bond, and O11, that has no such interaction, the sum is higher. The distance of the lone pair to the O atom increases with decreasing density. Whether these tendencies are generally valid cannot be decided from these few observations and more data are needed for a deeper understanding.

6. Conclusions

In this study a topological analysis of the experimental charge density $\rho(\mathbf{r})$ could be performed on a hexapeptide molecule of 71 atoms. The experiment makes use of highly intense X-ray radiation (synchrotron or rotating anode) and area detection.

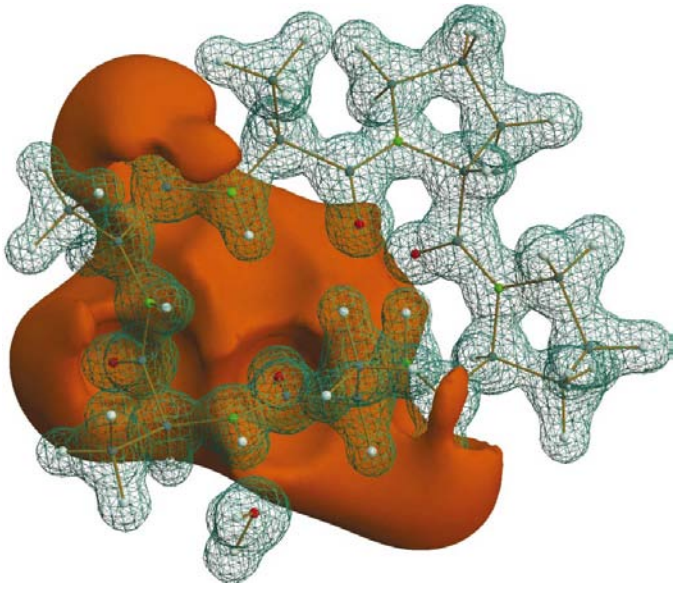

Figure 4
Electrostatic potential (synchrotron data), isosurfaces with 0.6 (turquoise) and −0.18 e Å^{-1} (orange).

Table 5
Non-bonded valence shell charge concentration of O atoms (synchrotron data).

	$\rho(\mathbf{r}_{CP})$	R	$\nabla^2\rho(\mathbf{r}_{CP})$	C—O—CP	CP_1—O—CP_2
O11	6.58	0.338	−150.2	106.1	–
	6.41	0.339	−148.7	97.8	155.6
O21	6.31	0.340	−131.5	106.6	–
	6.30	0.340	−129.7	119.8	133.5
O31	6.29	0.340	−144.2	110.5	–
	6.57	0.338	−147.8	105.6	142.0
O41	6.65	0.338	−155.2	111.7	–
	6.44	0.339	−135.0	95.3	152.5
O51	6.71	0.337	−162.0	117.5	–
	6.17	0.341	−127.2	108.2	127.3
O61	6.55	0.339	−135.4	115.5	–
	6.16	0.340	−136.5	113.2	127.3
O71	6.61	0.337	−154.7	102.7	–
	6.02	0.343	−119.1	140.1	87.4

R is the radial distance of the (3,+3) critical point (CP) of the Laplacian from the oxygen atom, C—O—CP is the angle formed by the C—O bond and the O—CP vector, CP_1—O—CP_2 is the angle formed by the CP_1—O and O—CP_2 vectors. $\rho(\mathbf{r}_{CP})$ is in e Å^{-3}, $\nabla^2\rho(\mathbf{r}_{CP})$ in e Å^{-5}.

Two datasets using a different experimental setup were compared. The quantitative results allow one to judge about the reproducibility of studies of this kind.

This study is one of the first of its kind on a larger oligopeptide (Abramov *et al.*, 2000; Jelsch *et al.*, 1998, 2000; Wiest *et al.*, 1994). The molecule is a suitable model compound for the backbone of a peptide as no other functional groups or charged terminal groups that would influence the charge distribution exist. As oligopeptides rarely form crystals of a quality that is suitable for a charge density study, the experimental characterization of the atomic interactions in the peptide bonds is especially valuable.

A good agreement between topological properties for the side chains has been found. This might have an interesting application for modelling the electron density of larger peptides from fragments defined according to Bader's theory.

This work was funded from BMBF, Verbund 47, Förderkennzeichen 05 SM8KEA0, the Deutschen Forschungsgemeinschaft DFG, Förderkennzeichen LU 222/22-1/2 and SCHE 487/2-1 and from the Fonds der Chemischen Industrie.

References

Abramov, Y. A., Volkov, A., Wu, G. & Coppens, P. (2000). *Acta Cryst.* A**56**, 585–591.
Bader, R. F. W. (1994). *Atoms in Molecules: A Quantum Theory*, No. 22 in The International Series of Monographs on Chemistry, 2nd ed. Oxford: Clarendon Press.
Bader, R. F. W. & Bayles, D. (2000). *J. Phys. Chem. A*, **104**, 5579–5589.
Benabicha, F., Pichon-Pesme, V., Jelsch, C., Lecomte, C. & Khmou, A. (2000). *Acta Cryst.* B**56**, 155–165.
Blessing, R. H. (1995). *Acta Cryst.* A**51**, 33–38.
Bruker AXS Inc. (1994–1996). *ASTRO, SMART, SAINT*. Technical Report. Bruker AXS Inc., Madison, Wisconsin, USA.
Burnett, M. N. & Johnson, C. K. (1996). *ORTEP*III. Report ORNL-6895. Oak Ridge National Laboratory, Tennessee, USA.
Chang, C. & Bader, R. F. W. (1992). *J. Phys. Chem.* **96**, 1654–1662.

Cheeseman, J., Keith, T. A. & Bader, R. F. W. (1992). *AIMPAC Program Package*. McMaster University, Hamilton, Ontario, Canada.
Clementi, E. & Roetti, C. (1974). *At. Nucl. Data Tables*, **14**, 177–478.
Dahaoui, S., Jelsch, C., Howard, J. A. K. & Lecomte, C. (1999). *Acta Cryst.* B**55**, 226–230.
Dittrich, B., Flaig, R., Koritsánszki, T., Krane, H.-G., Morgenroth, W. & Luger, P. (2000). *Chem. Eur. J.* **6**, 2582–2589.
Espinosa, E., Molins, E. & Lecomte, C. (1998). *Chem. Phys. Lett.* **285**, 170–173.
Flaig, R., Koritsánszky, T., Dittrich, B., Wagner, A. & Luger, P. (2002). *J. Am. Chem. Soc.* **124**, 3407–3417.
Flaig, R., Koritsánszky, T., Janczak, J., Krane, H.-G., Morgenroth, W. & Luger, P. (1999). *Ang. Chem. Int. Ed.* **38**, 1397–1400.
Frisch, M. J., Trucks, G. W., Schlegel, H. B., Scuseria, G. E., Robb, M. A., Cheeseman, J. R., Zakrzewski, V. G., Montgomery, J. A., Stratmann, R. E., Burant, J. C., Dapprich, S., Millam, J. M., Daniels, A. D., Kudin, K. N., Strain, M. C., Farkas, O., Tomasi,J., Barone, V., Cossi, M., Cammi, R., Mennucci, B., Pomelli, C., Adamo, C., Clifford, S., Ochterski, J., Petersson, G. A., Ayala, P. Y., Cui, Q., Morokuma, K., Malick, D. K., Rabuck, A. D., Raghavachari, K., Foresman, J. B., Cioslowski, J., Ortiz, J. V., Stefanov, B. B.,Liu, G., Liashenko, A., Piskorz, P., Komaromi,I., Gomperts, R., Martin, R. L., Fox, D. J., Keith, T., Al-Laham, M. A., Peng, C. Y., Nanayakkara, A., Gonzalez, C., Challacombe, M., Gill, P. M. W., Johnson, B., Chen, W., Wong, M. W., Andres, J. L., Gonzalez, C., Head-Gordon, M., Replogle, E. S. & Pople, J. A. (1998). *GAUSSIAN*98. Revision A.7. Gaussian Inc., Pittsburgh, PA, USA.
Gatti, C., Bianchi, R., Destro, R. & Merati, F. (1992). *J. Mol. Struct. (Theochem.)* **255**, 409–433.
Hansen, N. K. & Coppens, P. (1978). *Acta Cryst.* A**34**, 909–921.
Hirshfeld, F. L. (1976). *Acta Cryst.* A**32**, 239–244.
Jelsch, C., Pichon-Pesme, V., Lecomte, C. & Aubry, A. (1998). *Acta Cryst.* D**54**, 1306–1318.
Jelsch, C., Teeter, M. M., Lamzin, V., Pichon-Pesme, V., Blessing, R. H. & Lecomte, C. (2000). *Proc. Natl Acad. Sci.* **97**, 3171–3176.
Koritsánszky, T., Flaig, R., Zobel, D., Krane, H.-G., Morgenroth, W. & Luger, P. (1998). *Science*, **279**, 356–358.
Koritsánszky, T., Howard, S., Richter, T., Su, Z. W., Mallinson, P. R. & Hansen, N. K. (1995). *XD*. User Manual. Freie Universität Berlin, Berlin, Germany.
Nonius BV (2000). *EVAL Data Reduction Program.* Technical Report. Nonius BV, The Netherlands.
Pichon-Pesme, V., Lachekar, H., Souhassou, M. & Lecomte, C. (2000). *Acta Cryst.* B**56**, 728–737.
Pichon-Pesme, V. & Lecomte, C. (1998). *Acta Cryst.* B**54**, 485–493.
Popelier, P. L. A. & Bader, R. F. W. (1994). *J. Phys. Chem.* **98**, 4473–4481.
Sheldrick, G. M. (1997). *SHELXL*. University of Göttingen, Germany.
Spackman, M. A. (1999). *Chem. Phys. Lett.* **301**, 425–429.
Spek, A. L. (1990). *Acta Cryst.* A**46**, C34.
Wagner, A., Flaig, R., Koritsánszky, T. & Luger, P. (2000). *Z. Kristallogr.*, Suppl. Issue, **17**, 78.
Wiest, R., Pichon-Pesme, V., Bénard, M. & Lecomte, C. (1994). *J. Phys. Chem.* **98**, 1351–1362.